1

Introduction

1.1 Wetting fundamentals

The wetting of solid surfaces by a liquid plays a considerable role in biology, daily life and industry (Marmur, 1992b). In many processes and applications, which are applied in chemical, metallurgy, ceramic, petrochemical, pharmaceutical and food industry, the wettability decides about the quality or the success of the outcome. For instance, in the field of solids process engineering, the wettability of a particulate system is an important step during agglomeration, granulation or coating processes which can decide about the product quality (Charles-Williams et al., 2013, Hapgood et al., 2003, Iveson et al., 2001). Hence, an overview about fundamentals of wetting of a flat surface, a single capillary and a porous system is provided in this chapter.

1.1.1 Droplet spreading

When a liquid droplet gets in contact with a flat solid surface, two cases can be distinguished: total wetting and partial wetting. Sometimes even a third case is described, the partial nonwetting (Masoodi and Pillai, 2012). The three different wetting cases are presented in Figure 1.1.

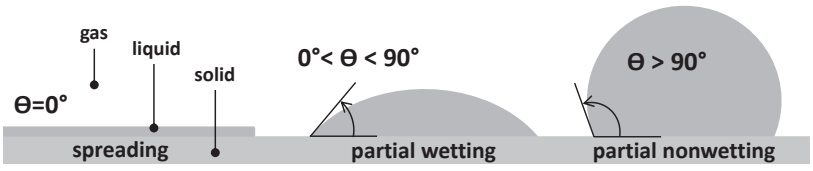

FIGURE 1.1: Three wetting cases: spreading, partial wetting and partial nonwetting.

In order to characterize the wettability, the spreading parameter Sp, which measures the difference between the surface energies of the substrate in a dry E_{dry} and in a wetted state E_{wet} (Eq. 1.1), is consulted. It can also be expressed by the surface tensions at the solid/air $\sigma_{s,g}$, solid/liquid $\sigma_{s,l}$ and liquid/air interfaces σ (Eq. 1.2) (de Gennes et al., 2004):

$$Sp = E_{dry} - E_{wet}, \tag{1.1}$$

$$Sp = \sigma_{s,g} - (\sigma_{s,l} + \sigma). \tag{1.2}$$

$Sp > 0$ means that the liquid spreads over the solid surface due to a strong affinity and to lower its surface energy. The resulting contact angle θ which forms at the three-phase boundary point is zero. The partial wetting is expressed by $Sp < 0$ and $\theta < 90°$ whereas the partial nonwetting is defined as $Sp < 0$ and $\theta > 90°$. Thus, besides the spreading parameter, the contact angle provides an opportunity to express the interactions between a solid and a liquid. Young (1805) defined the intrinsic contact angle on a molecular level which is based on a force balance (Eq. 1.3):

$$\sigma \cdot \cos\theta = \sigma_{s,g} - \sigma_{s,l}. \tag{1.3}$$

Since this contact angle can be only measured on ideal, flat, smooth and homogeneous surfaces, the apparent contact angle is observable on a microscopic level due to surface imperfections, reactions between fluid and solid material, roughness or chemical heterogeneity (Marmur, 1992a, Palzer et al., 2001, Reinke et al., 2015). These chemical and physical irregularities form non-ideal surfaces resulting in the fact that the static contact angle is not longer unique for the dynamic case (de Gennes et al., 2004, Li and Neumann, 1992). When a liquid droplet moves along a real solid surface, the contact angle varies between a maximum and a minimum value, which are termed as advancing θ_{ad} and receding contact angel θ_{rec}, respectively. The advancing contact angle is larger than the static value and occurs when a droplet is inflated and advances across a dry solid surface. On the contrary, when deflating a droplet the liquid recedes from the surface resulting in the smaller receding contact angle (de Gennes et al., 2004, Li and Neumann, 1992). The difference between the maximum and minimum contact angles is called the contact angle hysteresis. On clean and smooth surfaces, the hysteresis can be smaller than 5°, while rough and dirty surfaces can extend the hysteresis to more than 50° (de Gennes et al., 2004). The dynamic contact angle depends on the velocity of the contact line, but is indenpendent of the fact if it is a two-dimensional meniscus or a axisymmetric droplet (Katoh et al., 2010, 2015). In literature, different correlations are

available to describe the velocity dependence of the contact angle. Cox (1986) derived the following equation (Eq. 1.4), where θ_d is the dynamic contact angle, G is an experimental constant, Ca is the capillary number, L is the typical lengthscale of the system, L_{slip} is the slip length, η is the viscosity, u is the velocity and σ is the surface tension:

$$\theta_d = \left(\theta^3 + 9 \cdot G \cdot Ca\right)^{1/3}, \tag{1.4}$$

with

$$G = \ln\left(\frac{L}{L_{slip}}\right),$$
$$Ca = \frac{\eta \cdot u}{\sigma}.$$

Katoh et al. (2010) presented another approach (Eq.1.5) to express the dynamic contact angle, where e is the ratio occupied by defects:

$$|\cos\theta_d - \cos\theta| = \frac{3 \cdot (1-e)}{e \cdot \tan\theta_d} \cdot Ca. \tag{1.5}$$

As already mentioned above, surface heterogeneities are generally divided into two groups, physical and chemical heterogeneities. Contact angles on chemically heterogeneous, but smooth surfaces can be expressed by an approach presented by Cassie and Baxter (1944). Assuming the surface consists of two components, component 1 and 2, Figure 1.2 presents the composition of the Cassie-Baxter contact angle.

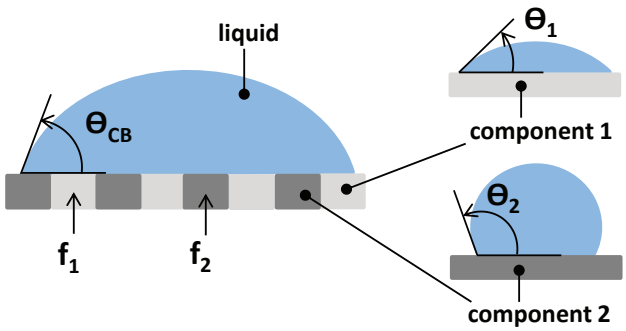

FIGURE 1.2: Cassie-Baxter contact angle θ_{CB} on chemical heterogeneous surface consisting of component 1 with θ_1 and component 2 with θ_2.

Eq.(1.6) can be applied to calculate the Cassie-Baxter contact angle θ_{CB} of two components. θ_1 and f_1 are the contact angle and the area surface fraction of component 1

and θ_2 and f_2 are the contact angle and the area surface fraction of component 2. The angle θ_{CB} appears as the apparent contact angle on the heterogeneous surface:

$$\cos\theta_{CB} = f_1 \cdot \cos\theta_1 + f_2 \cdot \cos\theta_2. \tag{1.6}$$

Physical heterogeneity on surfaces occurs due to geometric roughness which also influences the contact angle. This phenomenon of contact angles on rough, but chemical homogeneous surfaces was explained by Wenzel (1936, 1949). Eq. (1.7) presents the relation between the apparent contact angle, the roughness parameter R and the intrinsic contact angle:

$$\cos\theta_a = R \cdot \cos\theta_i, \tag{1.7}$$

with

$$R = \frac{\text{actual surface area}}{\text{geometric surface area}}.$$

Wenzel's relation describes the effect that roughness decreases the apparent contact angles if it is below 90° and increases the apparent contact angle if it is above 90° which can be seen in Figure 1.3.

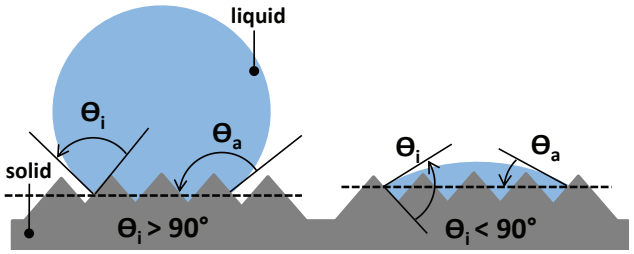

FIGURE 1.3: Effect of surface roughness on apparent contact angle θ_a for the two cases for the intrinsic contact angle θ_i: $\theta_i > 90°$ and $\theta_i > 90°$, modified from (Dullien, 1992).

This effect was experimentally confirmed by other authors (Busscher et al., 1984, Palzer et al., 2001) for the static case. Furthermore, Busscher et al. (1984) figured out that there is no influence of surface roughness on the contact angle as long as the roughness is below 0.1 µm. For the dynamic case, Palzer et al. (2001) generally observed higher contact angles with an increased surface roughness independent of the magnitude of the contact angle.

1.1.2 Liquid imbibition into single pore

Capillarity describes the behaviour of liquids in small tubes, called capillaries, due to interfacial forces. The capillary pressure P_{cap} is the driving force which pulls the liquid into the tubes (Masoodi and Pillai, 2012). r_p is the radius of the pore. Generally, it can be distinguished between two cases. If adhesion forces between liquid and capillary wall are larger than cohesion forces within the liquid, capillary rise can be observed. In the opposite case, capillary depression occurs (Dobrinski et al., 2010). A critical contact angle of 90° is the limiting case. Solid-liquid systems, which form contact angles below 90° result in capillary rise:

$$P_{cap} = \frac{2 \cdot \sigma \cos\theta}{r_p}. \tag{1.8}$$

During the penetration of liquid into a single capillary, different forces act in different directions and decide about the dynamics of the rise. The overall force balance is described by several authors in literature (Marmur, 1992a, Martic et al., 2002, Zhmud et al., 2000) and includes the capillary force F_{cap}, the viscous force F_{vis}, the gravity force F_{gr} and the inertial force F_{in} (Eq.(1.9):

$$F_{cap} = F_{vis} + F_{gr} + F_{in}. \tag{1.9}$$

Converting the force balance into a pressure balance by relating the forces to the cross-sectional area of the capillary or pore, Eq. (1.10) is obtained. The equation consists of four pressure terms, the capillary pressure, the hydrostatic pressure, the viscous pressure loss which is expressed in the Hagen-Poiseuille equation and the inertia term. r_p is the radius of the capillary or pore, ρ_l is the density of the liquid, g is the gravitational acceleration, h is the height and t is the time. In order to describe the rise into inclined capillaries as well, Fries and Dreyer (2008a) added the term $\sin\chi$ to the hydrostatic pressure where χ is the angle which forms between inclined capillary and free liquid surface:

$$\frac{2 \cdot \sigma \cdot \cos\theta}{r_p} = \frac{8 \cdot \eta \cdot h}{r_p^2} \cdot \frac{dh}{dt} + \rho_l \cdot g \cdot h \cdot \sin\chi + \rho_l \cdot \left[h \cdot \frac{d^2h}{dt^2} + \left(\frac{dh}{dt} \right)^2 \right]. \tag{1.10}$$

During the penetration of a liquid into a capillary, different effects are dominant depending on the time stage. Four cases can be distinguished (Fries and Dreyer, 2008b): the purely inertial time stage, the visco-inertial time stage, the purely viscous time stage and the viscous and gravitational time stage. A final stage is added, which describes the equilibrium state of liquid in a capillary.

Inertial time stage

Quéré (1997) presented the following approach for the very first moments when the liquid gets in contact with the capillary. During this time stage, the viscous and the gravity term can be neglected. Eq. (1.11) is the simplified version of Eq. (1.10):

$$\frac{2 \cdot \sigma \cdot \cos\theta}{r_p \cdot \rho_l} = h \cdot \frac{d^2h}{dt^2} + \left(\frac{dh}{dt}\right)^2. \tag{1.11}$$

The differential equation was solved by Quéré (1997) leading to a linear law for the meniscus height in a capillary versus time (Eq. 1.12):

$$h = t \cdot \sqrt{\frac{2 \cdot \sigma \cdot \cos\theta}{\rho_l \cdot r_p}}. \tag{1.12}$$

Visco-inertial time stage

Is the penetration dominated by viscous and inertial forces, Bosanquet (1923) derived the following simplification to express the behaviour of the flow (Eq.1.13):

$$h^2 = \frac{2b}{a} \cdot \left[t - \frac{1}{a} \cdot \left(1 - e^{-at}\right)\right], \tag{1.13}$$

with

$$a = \frac{8 \cdot \eta}{r_p^2 \cdot \rho_l},$$
$$b = \frac{2 \cdot \sigma \cdot \cos\theta}{r_p \cdot \rho_l}.$$

Eq. (1.13) transforms into the Washburn equation for $t \to \infty$. Ichikawa and Satoda (1994) studied the same case, but expressed the equation in a dimensionless form.

Viscous time stage

The viscous time stage during capillary rise is the most known and discussed case in literature. Neglecting the inertial and gravity forces Eq. (1.10) can be simplified and written as:

$$\frac{2 \cdot \sigma \cdot \cos\theta}{r_p} = \frac{8 \cdot \eta \cdot h}{r_p^2} \cdot \frac{dh}{dt}. \tag{1.14}$$

Solving Eq. (1.14) by inserting the initial condition $h(t = 0) = 0$ results in Eq. (1.15). This equation was derived by Washburn (1921) and Lucas (1918) independently from each other. But in the following the equation is titled as the Washburn equation:

$$h(t) = \sqrt{\frac{r_p \cdot \sigma \cdot \cos\theta}{2 \cdot \eta} \cdot t}. \tag{1.15}$$

The Washburn equation provides a basis for many modelling approaches of capillary rise phenomena in literature. This aspect is discussed more detailed in subsection 1.3.1.

Viscous and gravitational time stage

In the fourth stage, the penetration flow starts to be influenced by the gravity. Fries and Dreyer (2008a) figured out that the critical height when gravity has to be considered is at $h > 0.1 \cdot h_{eq}$, where h_{eq} is the equilibrium height in a capillary. Only the inertia effects can be neglected during this stage. An analytical solution is provided by using the Lambert function W for mathematical rearrangement (Eq. 1.16). a and b are constant factors including all solid and liquid properties and the gravity:

$$h(t) = \frac{a}{b}\left[1 + W\left(-e^{-1-\frac{b^2 \cdot t}{a}}\right)\right]. \tag{1.16}$$

Equilibrium stage

The equilibrium state is reached when the capillary pressure is balanced by the hydrostatic pressure (Eq. 1.18):

$$\frac{2 \cdot \sigma \cdot \cos\theta}{r_p} = \rho_l \cdot g \cdot h \cdot \sin\psi. \tag{1.17}$$

Assuming a vertical capillary ($\psi = 0$), the equilibrium height can be calculated with the following equation:

$$h_{eq} = \frac{2 \cdot \sigma \cdot \cos\theta}{\rho_l \cdot g \cdot r_p}. \tag{1.18}$$

Several other approaches are available in literature dealing for instance with short and long term solutions for the prediction of capillary rise (Chebbi, 2007, Zhmud et al., 2000) or with the influence of dynamic contact angles on the penetration behaviour (Chebbi, 2007, Hamraoui et al., 2000, Siebold et al., 2000).

Another influencing factor is the shape of the pore. Most studies assume cylindrical pores in which the liquid is imbibed. Birdi et al. (1988) and Wu et al. (2016) derived empirical equations for calculating the equilibrium height in rectangular capillaries. While the equation of Birdi et al. (1988) can be only applied for solid-liquid systems forming a contact angle of 0, Wu et al. (2016) included a term for the contact angle. Liquid penetration in angular gaps was studied by Bico and Quere (2002) for homogeneous square tubes and by O'Brien et al. (1968) for dissimilar walls with an angle.

O'Brien et al. (1968) developed a mathematical model to predict the capillary penetration between dissimilar plates (Eq. 1.19). The equation was evaluated with experiments which were conducted for different liquids between heterogeneous systems, such as glass-Teflon and glass-acrylic resin. The advancing contact angles of the materials were measured to be 14°, 74° and 110° for glass, acrylic and Teflon, respectively:

$$h_{eq} = \frac{\sigma \cdot (\cos\theta_1 + \cos\theta_2)}{\rho_l \cdot g \cdot w}. \tag{1.19}$$

In order to compare their measured data with the modelled rise, they used the factor $w \cdot h_{eq}$, which is the product of the gap width w multiplied by the equilibrium height. The deviation of the mean observed values from the predicted values is 2 % for the glass-acrylic system and 21 % for the glass-Teflon system.

1.1.3 Penetration into pore network

Capillary penetration into a pore network within a powder bed is based on the same physical fundamentals as the wicking into a single pore, however, the shape and the orientation of pores changes dramatically in these pore networks. Thus, significant differences in the behaviour are the consequences. Raux et al. (2013) compared the wicking of water into a capillary glass tube and into a porous media made of glass beads. For three different wettabilities, the glass tubes and beads were treated equally to modify the surface resulting in contact angles of 35°, 70° and 105°. For the contact angle of 35°, a wicking could be observed into both systems and for the angle of 105°, no wicking occurred. While the water penetrated into the 70°-glass tube, no penetration happened in the bed of glass beads, even if the contact angle was below 90°. This

phenomenon was explained by geometrical reasons, since the pores within a powder bed are not cylindrical.

Nevertheless, a pore network within a powder bed is often described as a bundle of parallel cylinders with identical pore radii in literature which is also attributable to Washburn (1921). Therefore, in order to apply the Washburn equation for porous systems the pore radius r_p is replaced by an effective radius $r_{p,eff}$ of the parallel, cylindrical pores in Eq.(1.15). The following assumptions have to be made: 1. stationary, laminar flow, 2. no external pressure, 3. neglection of gravity force, 4. neglection of inertial force, 5. no-slip condition at the wall, 6. constant capillary pressure. Figure 1.4 presents a real powder bed and its model system.

The pore network can also be expressed as the product $k \cdot r_p$, where k is a constant to describe the randomly oriented capillaries (Bruil and van Aartsen, 1974). This product is determined by passing an ideal spreading liquid ($\theta = 0$) with known liquid parameters σ and η through the powder. Assuming a constant bed independent of the passing liquid this method is applicable (Rosen, 1978).

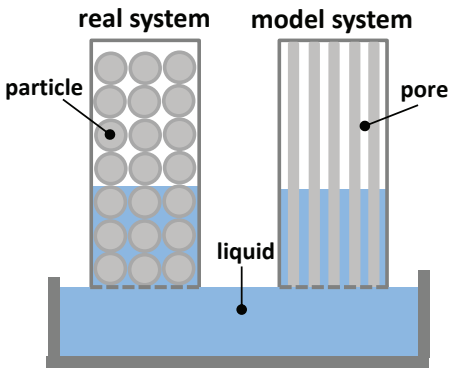

FIGURE 1.4: Real pore network (left) and model system (right) assuming a bundel of parallel, cylindrical pores (modified from Palzer (2000)).

Since the measurement of the liquid height for the Washburn approach is challenging, Murata and Naka (1983) and Kilau and Pahlman (1987) replaced the height by the penetration weight M_l of the liquid and used a modified equation (Eq. 1.20). An advantage of this modification is that the weight of the liquid uptake within the tube can be measured precisely, while the height of the liquid front is only visible at the glass wall of the tube but not in the interior. Therefore, the weight of the liquid within the tube is expressed by the height, the porosity ε of the powder bed, the cross sectional area of the tube A and the liquid density:

$$M(t) = \varepsilon \cdot A \cdot \rho_l \cdot \sqrt{\frac{k \cdot r_p \cdot \sigma \cos\theta}{2 \cdot \eta} \cdot t}. \tag{1.20}$$

The mass related Washburn equation can be also formulated differently (Eq. 1.21). Siebold et al. (1997) summarized the pore network parameters r_p, ε, A in the geometric factor K which is also obtained by using an ideal spreading liquid forming a contact angle of 0 on the solid. K is also called the capillary constant:

$$M(t) = \sqrt{\frac{K \cdot \rho_l^2 \cdot \sigma \cos\theta}{\eta} \cdot t}, \tag{1.21}$$

with

$$K = \frac{r_{p,eff} \cdot A^2 \cdot \varepsilon^2}{2}. \tag{1.22}$$

A critical step for this method is the creation of reproducible powder packings for the determination of K and the actual penetration experiment using the desired wetting liquid (Galet et al., 2010). Secondly, the correct choice of an ideal wetting liquid is decisive for this method (Prestidge and Ralston, 1995). Commonly used ideal wetting liquids are hexane, cyclohexane, heptane or octane (Chau, 2009, Galet et al., 2010, Iveson et al., 2000, Siebold et al., 1997, Susana et al., 2012).

Palzer (2000) presented another modified Washburn approach to describe the capillary wetting into a porous system. He suggested to use mercury porosimetry to get information about the real pore structure in the powder. Eq. (1.23) can be derived using the mean pore radius $r_{p,50}$ from the pore size distribution and introducing a shape factor ψ. This shape factor converts the real pore radius into an equivalent pore radius of the porous system by considering the deviation of the pore shape from the cylindrical shape and the alteration of the pore length due to curvature:

$$h(t) = \sqrt{\frac{r_{p,50} \cdot \psi \cdot \sigma \cdot \cos\theta}{2 \cdot \eta} \cdot t}. \tag{1.23}$$

If there is no possibility to measure the pore size distribution of a powder system, two further alternatives to determine pore radii in powder beds are proposed by Hapgood et al. (2002). The first approach was defined by White (1982) and contains the porosity ε, the mass specific surface area S_m and the solid density ρ_s (Eq. 1.24). A second approach (Eq. 1.25) is traced to Kozeny (1927) and Carman (1956) assuming approximately spherical particles with the Sauter diameter d_{32} and a shape factor ψ. The Wadell shape factor ψ_{Wa} can be inserted for ψ: